Ocean Engineering 196 (2020) 106817

Contents lists available at ScienceDirect

Ocean Engineering

journal homepage: www.elsevier.com/locate/oceaneng

Irregular frequency elimination of three-dimensional hydroelasticity in frequency domain

Peng Yang [a], Jingru Li [a,*], Dongwei Wu [b], Wei Zhang [c]

[a] Department of Mechanics and Electrics Engineering, Hainan University, No.58 Renmin Road, Meilan District, Haikou, 570228, China
[b] China Ship Development and Design Center, No. 268 Zhangzhidong Road, Wuchang District, Wuhan, 430064, China
[c] Guangdong Provincial Key Laboratory of Durability for Marine Civil Engineering, Shenzhen University, Shenzhen, 518060, China

ARTICLE INFO

Keywords:
Irregular frequency
Hydroelasticity
Green's function
Potential fluid
Boundary element method

ABSTRACT

The irregular frequencies affect the analysis of hydroelastic responses and wave loading of the floating structures, such as springing and whipping. In numerical prediction, the responses are likely to be overestimated. The theoretical basis of three-dimensional hydroelasticity for removing irregular frequencies in infinite and finite water depths is formed by a boundary integral method and adding a rigid lid to free surface of the inner fluid zone. One barge and one bulk carrier are taken as research objects for validating the feasibility of method for hydroelasticity and investigating the influence of the irregular frequency on hydrodynamic coefficients, diffraction forces and hydroelastic responses. The effectiveness of the method and mesh of the rigid lid are assessed. The method adopted in the paper could efficiently eliminate the irregular frequency for infinite and finite water depths. The irregular frequencies should be eliminated in a hydroelastic response assessment, especially for the large floating structures.

1. Introduction

Irregular frequencies correspond to the eigenfrequencies of the interior homogeneous Dirichlet problem (Ohmatsu, 1975) and affect the correctness of the solution, which have large influence on hydrodynamic coefficients, diffraction forces and motion responses in wave-body interaction analysis. The irregular frequency elimination of rigid floating structures in seakeeping is a traditional problem. There are many studies involving the irregular frequencies of rigid floating structures (Ohmatsu, 1975; Ursell, 1981.; Lee and Sclavounos, 1989; Zhu, 1994; Lee et al., 1996; Teng and Li, 1996; Du et al., 2011; Song and Teng, 2016). The extended integral equation is widely used for removing irregular frequencies (Lee and Sclavounos, 1989; Zhu, 1994; Lee et al., 1996). Another method is to modify the Green's function (Zhu, 1994). One new approach is the wall damping method (Liu and Falzarano, 2019), where the gap resonance in side-by-side offloading problems has been investigated by the method. A unique solvable higher-order BEM (boundary element method) for wave diffraction and radiation was investigated (Teng and Li, 1996). The occurrence of irregular frequencies in the numerical calculations of forward speed ship seakeeping has been studied (Du et al., 2011), indicating that there are few irregular frequencies in forward floating structures. An integral equation removing the irregular frequency was introduced into the pre-corrected FFT method for the wave-structure interaction (Song and Teng, 2016). The irregular frequency influences elastic response prediction, but few studies have considered irregular frequencies in hydroelastic mechanics. Some researchers have tried to eliminate irregular frequencies in a 3D hydroelastic analysis (Ni et al., 2019), and the studies indicated that the hydroelastic responses are influenced by irregular frequency effect. However, the detailed framework and deepening summary of the phenomenon have not been presented by considering hydroelasticity. Thus, it is necessary to form the framework of the fundamental theory and integral equation for eliminating irregular frequencies.

In the past two decades, floating structures have developed rapidly on a large scale. For example, the maximum volume of containers has increased from several thousand to more than 22,000 TEU. The springing of an ultra-large ore carrier with 500,000 DWT was investigated using the 3D second-order nonlinear hydroelastic method in the frequency domain (Hu et al., 2012). Furthermore, the nonlinear hydroelastic responses, springing and whipping of a large bulk carrier were studied by means of an inner and outer region matching method and model tests (Yang, 2016;Yang et al., 2018). A fully coupled time-domain solution for the hydroelastic analysis of a floating body was established (Pal et al., 2018). However, due to the emergence of large

* Corresponding author.
E-mail address: leslieljr@sina.com (J. Li).

https://doi.org/10.1016/j.oceaneng.2019.106817
Received 19 May 2019; Received in revised form 2 December 2019; Accepted 2 December 2019
Available online 18 December 2019

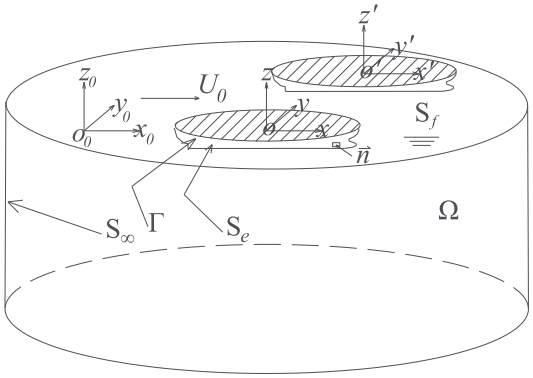

Fig. 1. Sketch of the coordinate systems.

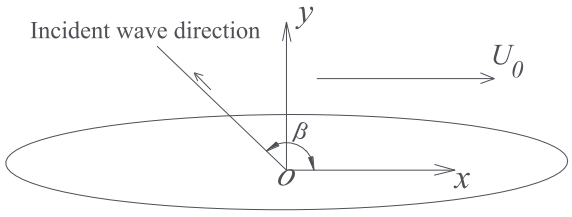

Fig. 2. Sketch of the wave direction.

offshore structures or multi-module floating structures, the hydroelastic method has been increasingly widely used. The hydroelasticity of very large floating structures in the presence of inhomogeneous sea conditions and unsteady external loads was investigated by an indirect time-domain method (Wei et al., 2018; Zhang et al., 2018). The contribution of wave energy generation devices and auxiliary buoys in reducing the hydroelastic responses of very large floating structures was studied (Nguyen et al., 2019). The hydroelastic responses of legged floating box structures were also studied by a numerical method and model tests (Wu et al., 2019). Thus, the development of hydroelastic mechanics is very important for marine structure and ocean engineering. And, there are also irregular frequency problems for the direct method in time domain, but specific solutions will not be studied in this paper.

Based on a potential fluid model and the superposition of structural elastic modes, extended integral equations of elastic floating structures with a forward speed are applied for three-dimensional hydroelastic mechanics. Assuming that the floating body moves slightly at its equilibrium position, the nonlinear free-surface condition is linearized. Under the assumption of a low speed and high frequency, the radiation potential and solution conditions of hydroelasticity in the three-dimensional frequency domain are simplified. Furthermore, the influence of the irregular frequency on hydrodynamic coefficients, diffraction forces and hydroelastic responses are investigated in hydroelastic mechanics. The effectiveness of the method in removing the irregular frequency is assessed for infinite and finite water depths.

2. Fundamental theory and mathematical formulation

2.1. Basic assumption

The fluid around an elastic ship hull is usually assumed to be uniform, incompressible, non-viscous, and non-rotating when studying the interaction between the floating structure and a wave; meanwhile, the effects of lift force and surface tension are not considered. On the other hand, the elastic deformation of the structure is considered to be small, and the overall response satisfies the linear superposition principle of the modal deformation.

2.2. Definition of the coordinate system

The ships straightly travel with a constant forward speed U_0. For convenience of the presentation, three coordinate systems are established as shown in Fig. 1, which are

(1) The space fixed coordinate system $O_0x_0y_0z_0$: the coordinate origin is located at the still water surface, the axis O_0x_0 points to the bow, the axis O_0y_0 points to the port side, and the axis O_0z_0 points upward perpendicular to the still water surface.
(2) The equilibrium coordinate system (also called the reference coordinate system) $Oxyz$: the coordinate system moves forward accompanying the ship along the x axis at a constant speed U_0, which coincides with the space-fixed coordinate system $O_0x_0y_0z_0$ in the initial moment. In addition, the axis Ox remains pointed towards the axis O_0x_0 during the ship motion.
(3) The local coordinate system $O'x'y'z'$: this coordinate system is fixed on the hull. When the hull is in the equilibrium position, this coordinate system overlaps with the equilibrium coordinate system. The origin position changes with the translational motion of the hull, and the direction changes with the rotation of the hull.

The fluid boundary is made up of a wetted body surface S_e, a free surface S_f, the intersection of the body surface and free surface Γ, and an infinite boundary S_∞. Ω denotes the fluid field. $\vec{n}$ denotes the normal direction of the body surface towards the inner zone of the ship hull. U_0 denotes the forward speed of the ship hull.

Both the space-fixed coordinate system and the equilibrium coordinate system obey the right-hand rule. Consider the following coordinate transformation relations.

$$\begin{cases} x_0 = x + U_0 t, y_0 = y, z_0 = z, \nabla_{x_0} = \nabla_x \\ \left.\dfrac{\partial}{\partial t}\right|_{x_0} \rightarrow \left.\dfrac{\partial}{\partial t}\right|_{x} - U_0 \left.\dfrac{\partial}{\partial x}\right|_{x} \end{cases} \tag{1}$$

The definition of the wave direction β shown in Fig. 2 with 0° and 180° denote the following sea and heading sea, respectively.

2.3. Decomposition of the velocity potential

When studying the motion of ocean structures in waves, the total velocity potential $\Phi(x_0, y_0, z_0, t)$ in the fixed coordinate system is usually decomposed into a wave-making velocity potential $\overline{\varphi}(x, y, z)$ and an unsteady velocity potential $\varphi(x, y, z, t)$. The velocity potential of the wave-making fluid field is generated by the floating structure sailing in still water. The unsteady velocity potential is constituted by incident potential, diffraction potential and radiation potential induced by the rigid motion and elastic deformation of the floating structures.

$$\Phi(x_0, y_0, z_0, t) = \widehat{\varphi}(x, y, z, t) = U_0\overline{\varphi}(x, y, z, t) + \varphi(x, y, z, t) \tag{2a}$$

Then, a new function $\widehat{\varphi}(x, y, z, t)$ is introduced, which is the velocity potential in the equilibrium coordinate system and satisfies the Laplace equation. In addition,

$$\frac{\partial \Phi}{\partial x_0} = \frac{\partial \widehat{\varphi}}{\partial x}, \frac{\partial \Phi}{\partial y_0} = \frac{\partial \widehat{\varphi}}{\partial y}, \frac{\partial \Phi}{\partial z_0} = \frac{\partial \widehat{\varphi}}{\partial z} \tag{2b}$$

$$\frac{\partial \Phi}{\partial t} = \left(\frac{\partial}{\partial t} - U_0\frac{\partial}{\partial x}\right)\widehat{\varphi} \tag{2c}$$

The unsteady velocity potential $\varphi(x, y, z, t)$ is decomposed into three parts.

$$\varphi(x, y, z, t) = \varphi_0(x, y, z, t) + \varphi_D(x, y, z, t) + \varphi_R(x, y, z, t) \tag{3}$$

where φ_0, φ_D and φ_R denote the incident potential, diffraction potential

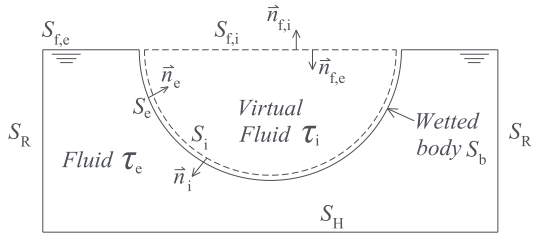

Fig. 3. A schematic diagram of the fluid field.

and radiation potential, respectively.

Furthermore, for a regular exciting wave $\zeta = e^{-i\omega_0 t}$, the relationship between the wave encounter frequency ω and wave frequency ω_0 is as follows:

$$\omega = \omega_0 - k_0 U_0 \cos\beta \tag{4}$$

where g denotes the gravitational acceleration and k_0 denotes the wavenumber corresponding to wave frequency ω_0.

The unsteady harmonic potential is expressed as (Wu, 1984). And,

$$\varphi(x,y,z,t) = \mathrm{Re}\left[\varphi(x,y,z)e^{-i\omega t}\right] \tag{5a}$$

where i denotes the imaginary unit. Re denotes a real part. φ represents φ_0, φ_D or φ_R. The expression of potential $\varphi_0(x,y,z)$ of the incident wave in finite water depth is

$$\varphi_0(x,y,z) = \frac{Ag}{i\omega_0}\frac{\cosh k_0(z+H)}{\cosh k_0 H}e^{ik_0(x\cos\beta + y\sin\beta)} \tag{5b}$$

where A and H denote the wave amplitude and water depth, respectively.

It is assumed that the motions and distortions of the floating structure in the waves are small and that the dynamic responses of the whole fluid-structure system are linear. According to the principle of linear superposition, the radiation potential φ_R is expressed as a superposition of the velocity potential corresponding to each normal (or natural) mode of the structure.

$$\varphi_R(x,y,z) = \sum_{r=1}^{\infty} -i\omega p_r \varphi_r(x,y,z) \tag{6}$$

where p_r (r = 1, 2, …, m) denotes the rth modal principal coordinate response. In particular, the variable r from 1 to 6, denotes the six rigid motions of the floating structure, namely, surge, sway, heave, roll, pitch and yaw, respectively.

The translational displacement $\vec{u}$ and rotation $\vec{\theta}$ at any position of the ship structure may be expressed as an aggregate of displacements in its principal modes (Wu, 1984; Price and Wu, 1984; Bishop et al., 1986).

$$\vec{u} = \sum_{r=1}^{m} \vec{u}_r p_r(t) = \sum_{r=1}^{m} (u_r, v_r, w_r) p_r(t) \tag{7a}$$

$$\vec{\theta} = \sum_{r=1}^{m} \vec{\theta}_r p_r(t) = \sum_{r=1}^{m} (\theta_{x,r}, \theta_{y,r}, \theta_{z,r}) p_r(t) \tag{7b}$$

where $\vec{u}_r = (u_r, w_r, v_r)$ and $\vec{\theta}_r = (\theta_{x,r}, \theta_{y,r}, \theta_{z,r})$ denote the translation and rotation of each structural node for the rth principal mode, respectively.

2.4. Control equation and boundary condition

Assuming that the floating body moves slightly at its equilibrium position, the nonlinear free-surface condition is linearized. Under the assumption of a low speed and high frequency ($i\omega - U_0\frac{\partial}{\partial x} \approx i\omega$), the radiation potential and solution conditions of hydroelasticity in the three-dimensional frequency domain are as follows. This method is called the "frequency domain method based on speed correction" for considering the forward speed effect. And the schematic diagram of the fluid field shown in Fig. 3.

Control equation in the fluid is

$$\nabla^2 \varphi_r(x,y,z) = 0 \tag{8a}$$

The boundary conditions on the free surface, the wetted body surface, seabed radiation and radiation condition are listed as follows, respectively.

$$\frac{\partial \varphi_r}{\partial z} - \nu\varphi_r = 0 \tag{8b}$$

$$\left.\frac{\partial \varphi_r}{\partial n}\right|_{S_b} = a_r + \frac{b_r}{\omega}i \tag{8c}$$

$$\lim_{z\to-\infty} \nabla\varphi_r = 0 \; or \left.\frac{\partial \varphi_r}{\partial z}\right|_{z=-H} = 0 \tag{8d}$$

$$\lim_{R\to\infty} \sqrt{R}\left(\frac{\partial \varphi_r}{\partial R} - ik\varphi_r\right) = 0 \tag{8e}$$

where $\vec{n}$ denotes the normal direction of the body surface. a_r and b_r denote the general boundary conditions of the rth mode of the elastic wetted body, respectively. H denotes the water depth. $\nu = \omega^2/g$. R denotes the radiation radius of the outer propagating wave. k denotes the wavenumber of encountering wave. S_b denotes the wetted surface of the floating structure.

In Fig. 3, τ_i and τ_e denote the virtual internal fluid field and actual external fluid field, respectively. The former is surrounded by S_i and $S_{f,i}$. The latter is surrounded by S_e, $S_{f,e}$, S_R and S_H. S_R denotes the infinite boundary surface of the wave radiation. S_H denotes the seabed. S_i and S_e denote the inner and outer surfaces of the wetted surface S_b of the floating body, respectively. The outside of S_e contacts with the actual fluid field. The corresponding unit normal vectors $\vec{n}_i$ and $\vec{n}_e$ denote the unit normal directions of S_i and S_e, respectively, which oppositely point in the directions of the external and internal fluid fields. $S_{f,i}$ and $S_{f,e}$ denote the free wave surfaces of the internal fluid field and the external fluid field, respectively. Additionally, the corresponding unit normal directions are $\vec{n}_{f,i}$ and $\vec{n}_{f,e}$, which point vertically upward and downward, respectively.

The generalized boundary condition of the radiation potential on the body's wetted surface may be represented as (Wu, 1984)

$$\frac{\partial \varphi_r}{\partial n} = (\vec{u}_r \cdot \vec{n})\dot{p}_r + [\vec{\theta}_r \times \vec{W} \cdot \vec{n} - (\vec{u}_r \cdot \nabla)\vec{W} \cdot \vec{n}]p_r \tag{9a}$$

where $\vec{n} = (n_1, n_2, n_3)$ denotes the unit normal vector. $\vec{W} = (W_x, W_y, W_z)$ denotes the velocity of the steady flow relative to the moving equilibrium coordinate system.

The Eq. (9a) can be simplified as

$$\frac{\partial \varphi_r}{\partial n} = a_r\dot{p}_r + b_r p_r \tag{9b}$$

and

$$a_r = \vec{u}_r \cdot \vec{n} \tag{9c}$$

$$b_r = \vec{\theta}_r \times \vec{W} \cdot \vec{n} - (\vec{u}_r \cdot \nabla)\vec{W} \cdot \vec{n} \tag{9d}$$

For a slender, thin, flat, or slowly moving body, The velocity of the steady flow may be simplified as $\vec{W} = (-U_0, 0, 0)$. In this case, the expression of b_r in Eq. (9d) can be written as (Wu, 1984)

$$b_r = -\frac{U_0}{2}\left[n_2\left(\frac{\partial v_r}{\partial x}-\frac{\partial u_r}{\partial y}\right)-n_3\left(\frac{\partial u_r}{\partial z}-\frac{\partial w_r}{\partial x}\right)\right]=U_0\left(n_3\theta_{yr}-n_2\theta_{zr}\right) \tag{9e}$$

or $b_r = U_0 m_r$, denoting $m_r = n_3\theta_{y,r} - n_2\theta_{z,r}$.

The boundary control equations and condition of the diffraction potential $\varphi_D(x,y,z)$ are the similar to the radiation case, except for the boundary condition Eq. (8c) on the wetted body, which is rewritten as

$$\left.\frac{\partial \varphi_D}{\partial n}\right|_{S_b} = -\frac{\partial \varphi_0}{\partial n} \tag{10}$$

The diffraction force of the rth mode induced by the diffraction potential is

$$F_{D,r} = \mathrm{i}\omega\rho \iint_{S_b} \varphi_D a_r \mathrm{d}S \tag{11a}$$

In addition, the incident force of the rth mode induced by the incident potential is

$$F_{I,r} = \mathrm{i}\omega\rho \iint_{S_b} \varphi_0 a_r \mathrm{d}S \tag{11b}$$

2.5. Hydrodynamic coefficients and response equation

For the harmonic exciting wave, the principal coordinate p_r in the frequency domain is derived and expressed as follows (Wu, 1984).

$$[a+A]\{\ddot{p}\}+[b+B]\{\dot{p}\}+[c+C]\{p\}=\{F\} \tag{12}$$

where $\{p\}$ denotes the principal coordinate. $[a]$, $[b]$ and $[c]$ are the inertia mass matrix, damping matrix and elastic restoring force matrix, respectively. $[A]$, $[B]$ and $[C]$ are the generalized added mass, added damping and restoring coefficient, respectively. $\{F\}$ denotes the generalized wave exciting force. The elements of these matrices are as follows (Wu, 1984; Du, 1996).

$$A_{rk} = \mathrm{Re}\left[\rho \iint_{S_b} a_r\varphi_k \mathrm{d}S + \rho U_0 \iint_{S_b} \vec{n}\frac{\partial \vec{u}_r}{\partial x}\varphi_k \mathrm{d}S\right] \tag{13a}$$

$$B_{rk} = \mathrm{Im}\left[\rho\omega \iint_{S_b} a_r\varphi_k \mathrm{d}S + \rho\omega U_0 \iint_{S_b} \vec{n}\frac{\partial \vec{u}_r}{\partial x}\varphi_k \mathrm{d}S\right] \tag{13b}$$

$$C_{rk} = \rho g \iint_{\bar{S}_b} a_r w_k \mathrm{d}S \tag{13c}$$

where Re and Im denote the real part and imaginary part, respectively. φ_k is the radiation potential of the kth mode. ρ denotes the fluid density.

2.6. Wet resonance frequency

When the ship is floating on a water surface and encounters harmonic excitation, its structural dynamic responses can contain contributions of different dry natural modes. At special exciting frequencies, there are structural resonances. The dry natural frequencies are in the vacuum and are changed by the added mass and hydrostatic restoring effect from the fluid. The wet resonance frequency of the rth mode of the elastic structure in the fluid can be calculated by Eq. (14). When the added mass varies with the exciting frequency and the off-diagonal element of the added mass matrix and the hydro-static restoring matrix is non-zero, the wet resonance frequency calculated by Eq. (14) is approximate.

$$f_r = \sqrt{\frac{c_{rr}+C_{rr}}{a_{rr}+A_{rr}}}\ \mathrm{rad/s} \tag{14}$$

3. Velocity potential integral equation for eliminating irregular frequencies

3.1. Definition of the irregular frequencies

For solving Eq. (8) (a) to 8 (e), the velocity potential integral equations of diffraction and radiation are based on either potential or source formulations (Zhu, 1994). The irregular frequencies correspond to the eigenfrequencies of the interior homogeneous Dirichlet problem (Ohmatsu, 1975). The solution of velocity potential φ can be either do not exist or are non-unique (Lee et al., 1996), and has singularity, that causes the hydrodynamic coefficients (Eq. (13a) and (13b) and the exciting force of diffraction (Eq. (11a)) have singularity. Thus, the hydrodynamic coefficients and exciting force of diffraction are influenced by the irregular frequencies.

For an arbitrary floating body, the irregular frequencies cannot be determined analytically. However, for some simple bodies, such as a rectangle barge, the velocity potential satisfies the homogeneous Dirichlet condition on the bottom as follows. B, L, and T denote the breadth, length and draft of the barge, respectively. The irregular frequencies ω of the barge are as follows (Wu, 1984; Zhu, 1994).

$$\omega^2 = gk\coth(kT), \qquad k=\left[\left(\frac{m\pi}{L}\right)^2+\left(\frac{n\pi}{B}\right)^2\right]^{1/2} \tag{15}$$

where $m,n = 1,2,\cdots$.

3.2. Green's function

The expressions of Green's function for an infinite water depth and a finite water depth (Wu, 1984; Newman, 1985, 1990) in the frequency domain are as follows.

(1) Infinite water depth

$$G(P(x,y,z),Q(\xi,\eta,\zeta)) = \frac{1}{r}+\frac{1}{r_1} + \mathrm{P.V.}\int_0^\infty \frac{2\nu}{k-\nu}e^{k(z+\zeta)}\mathrm{J}_0(kR)\mathrm{d}k + \mathrm{i}2\pi\nu e^{\nu(z+\zeta)}\mathrm{J}_0(\nu R) \tag{16a}$$

(2) Finite water depth

$$G(P(x,y,z),Q(\xi,\eta,\zeta)) = \frac{1}{r}+\frac{1}{r_2}+ \mathrm{P.V.}\int_0^\infty \frac{2(k+\nu)\mathrm{e}^{-kH}\cosh k(z+H)\cosh k(\zeta+H)}{k\sinh(kH)-\nu\cosh(kH)}\mathrm{J}_0(kR)\mathrm{d}k + \mathrm{i}\frac{2\pi(K+\nu)\mathrm{e}^{-KH}\sinh(KH)\cosh K(z+H)\cosh K(\zeta+H)}{\nu H+\sinh^2(KH)}\mathrm{J}_0(KR) \tag{16b}$$

where P.V. denotes the principle value integral. K denotes the wavenumber of the encountering wave, and $K\tanh(KH) = \nu$. $P(x,y,z)$ and $Q(\xi,\eta,\zeta)$ are the field point and source point, respectively. In addition, $R = \sqrt{(x-\xi)^2+(y-\eta)^2}$, $r = \sqrt{(x-\xi)^2+(y-\eta)^2+(z-\zeta)^2}$, $r_1 = \sqrt{(x-\xi)^2+(y-\eta)^2+(z+\zeta)^2}$, and $r_2 = \sqrt{(x-\xi)^2+(y-\eta)^2+(z+2H+\zeta)^2}$. k_n is the positive real root of the equation $k_\mathrm{n}\tan k_\mathrm{n}H+\nu=0$. $\mathrm{J}_0(kR)$ is the zero-order Bessel function of the first kind. $\frac{1}{r_1}$ and $\frac{1}{r_2}$ are the mirrors of $\frac{1}{r}$ about the still water surface and seabed, respectively.

3.3. Extended velocity potential integral equation

Since the irregular frequencies correspond to the eigenfrequencies of the interior Dirichlet problem, it is possible to place a rigid lid on the interior free surface to suppress the interior sloshing modes. This

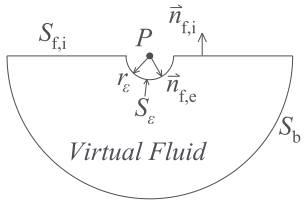

Fig. 4. Schematic diagram of the integral surrounding singularity.

Table 1
The principal parameters of the barge.

Parameters	Value
Length (m)	100.0
Broad (m)	25.0
Depth (m)	6.0
Draft (m)	2.5
Displacement Δ(t)	6350.0

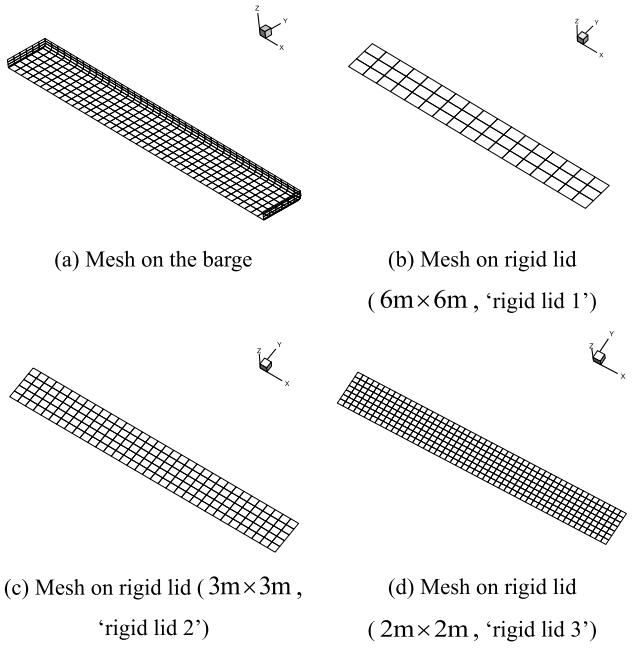

Fig. 5. Hydrodynamic model of the barge in the hydroelastic analysis (half model).

Table 2
The calculation case sets.

Name	Water depth	Rigid lid
'case1′	Infinite	No
'case2′		'rigid lid 3′
'case3′	10 m	No
'case4′		'rigid lid 1′
'case5′		'rigid lid 2′
'case6′		'rigid lid 3′

method has been derived by researchers (Ohmatsu, 1975; Kleiman, 1982).

For rigid floating structures in an infinite water depth, the extended boundary integral equation method for the removal of an irregular frequency has been deduced (Zhu, 1994; Lee et al., 1996). Herein, the methods for an irregular frequency elimination in 3D hydroelasticity for

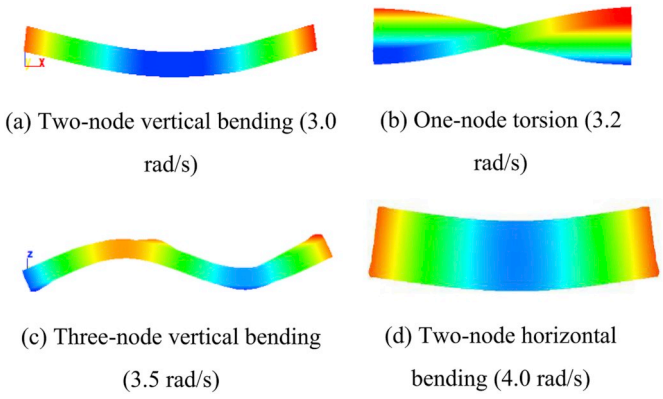

Fig. 6. Dry modal shapes of the barge.

Table 3
Dry natural frequencies and wet resonance frequencies.

Type	Dry natural frequency (rad/s)	Wet resonant frequency (rad/s)
Heave	–	0.95
Roll	–	1.12
Pitch	–	1.00
Two-node vertical bending ($f_{2\text{-VB}}$)	3.00	1.85
One-node torsion ($f_{1\text{-TN}}$)	3.20	2.45
Three-node vertical bending ($f_{3\text{-VB}}$)	3.50	2.15
Two-node horizontal bending ($f_{2\text{-HB}}$)	4.00	3.80

an infinite water depth and a finite water depth are presented as follows.

(1) Infinite water depth (Zhu, 1994)

$$G(P(x,y,z),Q(\xi,\eta,\zeta)) \approx \frac{1}{r}+\frac{1}{r_1}=\frac{2}{r} \tag{17a}$$

(2) Finite water depth

In the vicinity of the singular point on $S_{f,i}$, the fields $P(x,y,z)\to S_{f,i}$ and $Q(\xi,\eta,\zeta)\in S_{f,i}$; then, $z\to 0$ and $\zeta = 0$. Eq. (16b) can be rewritten as (Newman, 1984, Eq. (18); Newman, 1985, Eq. (11) ~ (13); Newman, 1990).

$$G(P(x,y,z),Q(\xi,\eta,\zeta)) \approx \left[\frac{1}{r}+\frac{1}{|2H-|z-\zeta||}+\frac{1}{|2H+|z-\zeta||}\right] + \left[\frac{1}{r_2}+\frac{1}{r_1}+\frac{1}{|4H+z+\zeta|}\right] \approx \frac{1}{r}+\frac{1}{r_1}=\frac{2}{r} \tag{17b}$$

When the field point P is coincident with the source point Q on the free surface, the integral at the singularity is shown in Fig. 4. S_ε and r_ε are the area and radius of the surface surrounding the singularity, respectively, and $r_\varepsilon \approx -z$.

φ_e and φ_i denote the velocity potential of the external surface and inner surface of the fluid boundary, respectively. One new variable $\sigma(Q)$ is introduced, and $\sigma(Q) = \frac{\partial\varphi_e(Q)}{\partial n_e} - \frac{\partial\varphi_i(Q)}{\partial n_e}$, called source strength. For the Green's function shown in Eqs. (16a) and (16b), when the field point $P(x,y,z)$ or the source point $Q(\xi,\eta,\zeta)$ is on the free surface, $\frac{\partial G}{\partial \zeta} = kG$. By combining the above formulas and taking, $\phi(P) = -k\varphi_i(P)$. The extended velocity potential integral equations can be given as

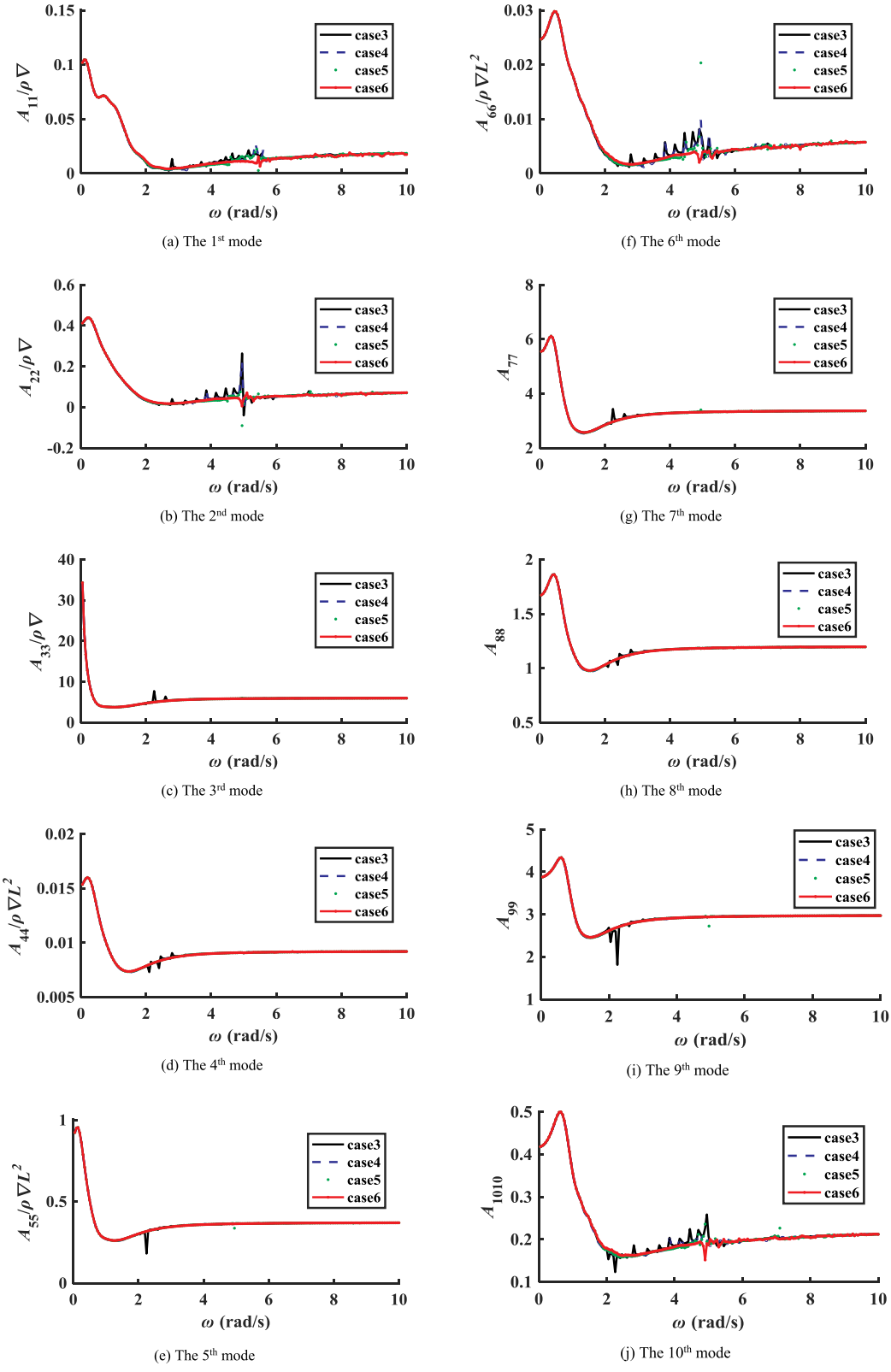

(a) The 1st mode
(b) The 2nd mode
(c) The 3rd mode
(d) The 4th mode
(e) The 5th mode
(f) The 6th mode
(g) The 7th mode
(h) The 8th mode
(i) The 9th mode
(j) The 10th mode

Fig. 7. Added mass of each mode (10 m water depth).

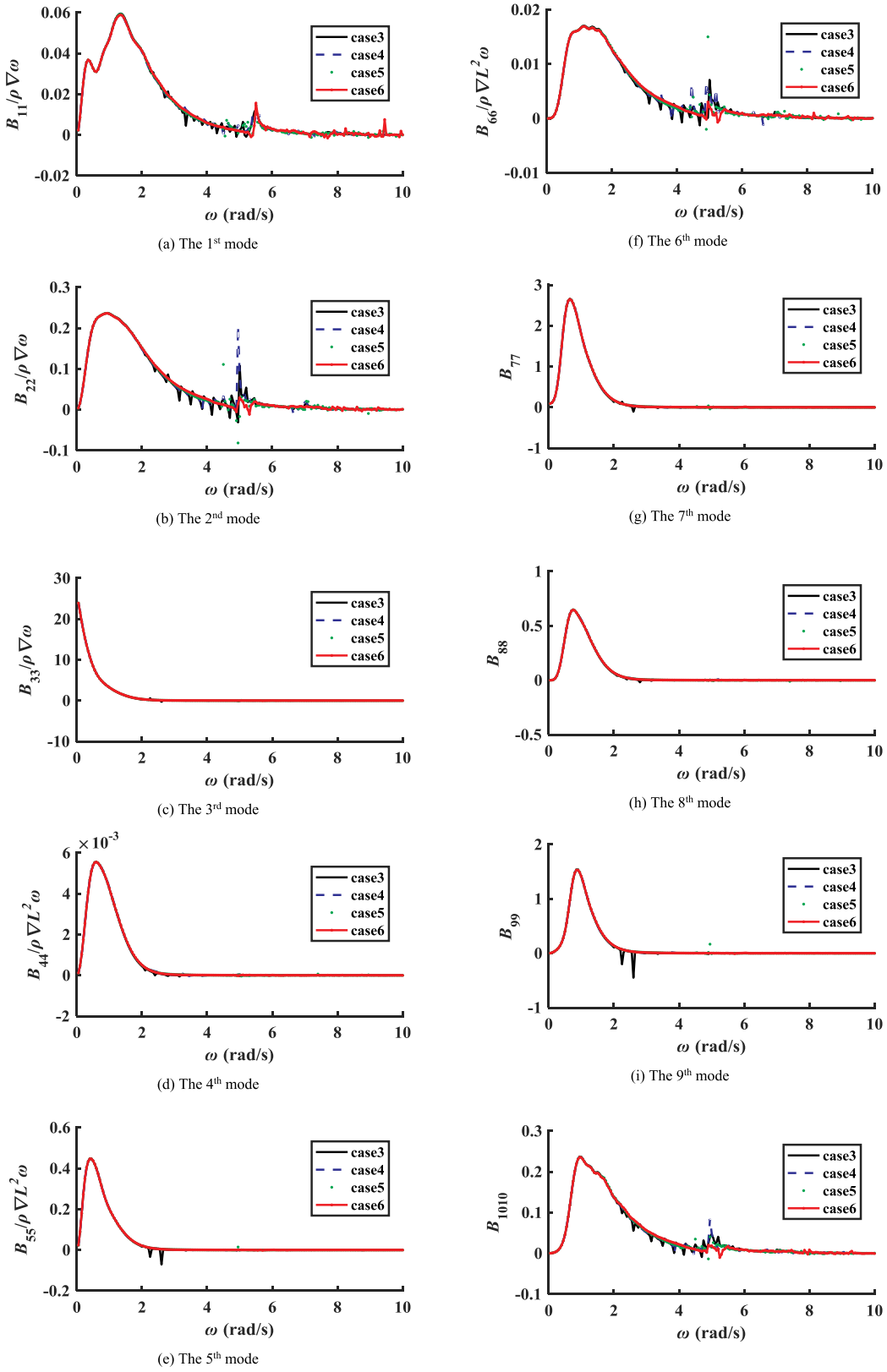

(a) The 1st mode
(b) The 2nd mode
(c) The 3rd mode
(d) The 4th mode
(e) The 5th mode
(f) The 6th mode
(g) The 7th mode
(h) The 8th mode
(i) The 9th mode

Fig. 8. Added damping of each mode (10 m water depth).

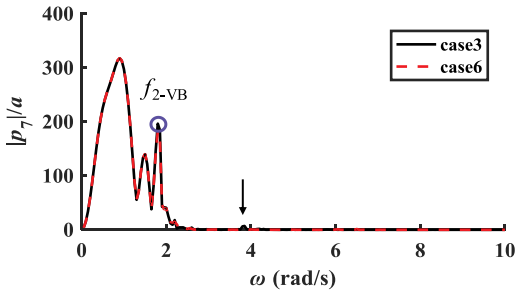

(a) The 7th mode

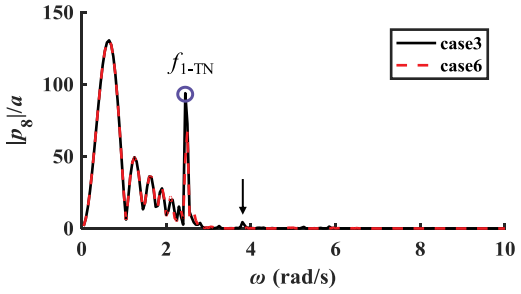

(b) The 8th mode

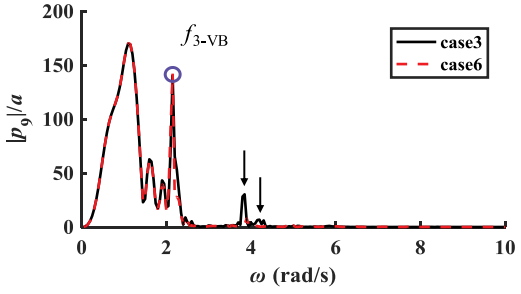

(c) The 9th mode

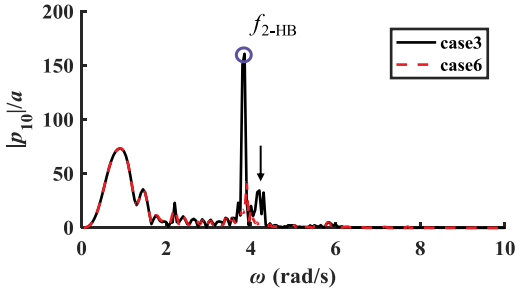

(d) The 10th mode

Fig. 9. The principal coordinate responses of the barge.

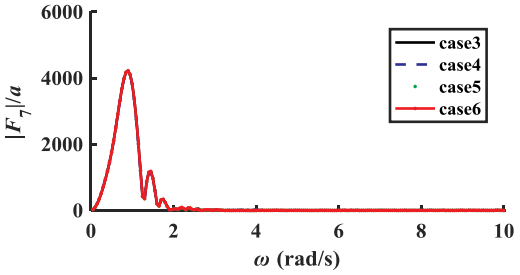

(a) The 7th mode

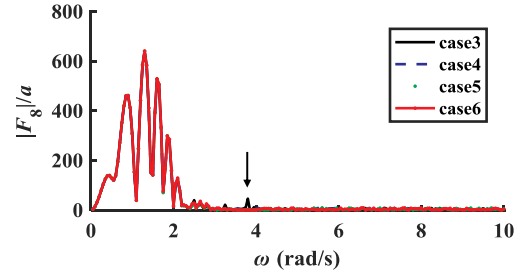

(b) The 8th mode

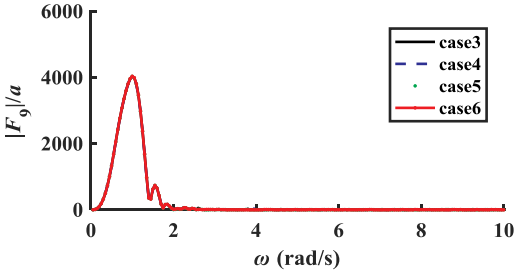

(c) The 9th mode

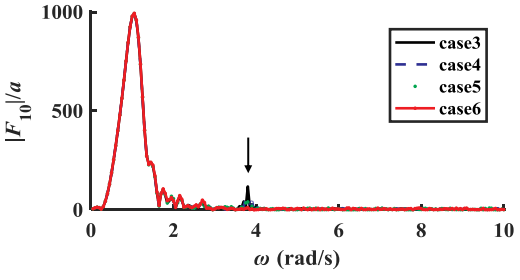

(d) The 10th mode

Fig. 10. Diffraction force of each mode (elastic modes, water depth of 10 m, wave direction of 45°).

$$\begin{cases} \dfrac{1}{4\pi}\iint_{S_e}\sigma(Q)\mathrm{G}(P,Q)\mathrm{d}S+\dfrac{1}{4\pi}\iint_{S_{\mathrm{f,i}}}\phi(Q)\mathrm{G}(P,Q)\mathrm{d}S \\ \qquad =\varphi(P), \quad P\in\tau_{\mathrm{e}}\cup\tau_{\mathrm{i}}\cup S_e \\ \dfrac{1}{4\pi}\iint_{S_e}\sigma(Q)\mathrm{G}(P,Q)\mathrm{d}S+\dfrac{1}{4\pi}\iint_{S_{\mathrm{f,i}}}\phi(Q)\mathrm{G}(P,Q)\mathrm{d}S \\ \qquad =-\dfrac{1}{k}\phi(P), \quad P\in S_{\mathrm{f,i}} \end{cases} \tag{18}$$

Furthermore, Eq. (18) is derived on both sides of the normal direction $n_{\mathrm{e}}(P)$. Using the rigid condition of the free surface $S_{\mathrm{f,i}}$: $V_{\mathrm{f,i}}=\frac{\partial\varphi_{\mathrm{i}}(Q)}{\partial n_{\mathrm{f,i}}}=0$, it is concluded that

$$\frac{1}{2}\sigma(P)+\frac{1}{4\pi}\iint_{S_e}\sigma(Q)\frac{\partial\mathrm{G}(P,Q)}{\partial n_{\mathrm{e}}(P)}\mathrm{d}S+\frac{1}{4\pi}\iint_{S_{\mathrm{f,i}}}\phi(Q)\frac{\partial\mathrm{G}(P,Q)}{\partial n_{\mathrm{e}}(P)}\mathrm{d}S=\frac{\partial\varphi(P)}{\partial n_{\mathrm{e}}(P)},P\in\tau_{\mathrm{e}}\cup\tau_{\mathrm{i}}\cup S_{\mathrm{e}} \tag{19a}$$

$$\frac{1}{4\pi}\iint_{S_e}\sigma(Q)\frac{\partial\mathrm{G}(P,Q)}{\partial n_{\mathrm{e}}(P)}\mathrm{d}S-\varphi_{\mathrm{i}}(P)+\frac{1}{4\pi}\iint_{S_{\mathrm{f,i}}}\phi(Q)\frac{\partial\mathrm{G}(P,Q)}{\partial n_{\mathrm{e}}(P)}\mathrm{d}S=-\frac{1}{k}\frac{\phi(P)}{\partial n_{\mathrm{e}}(P)}=0,P\in S_{\mathrm{f,i}} \tag{19b}$$

where the source strength $\sigma(Q)$ of the wetted surface and the source

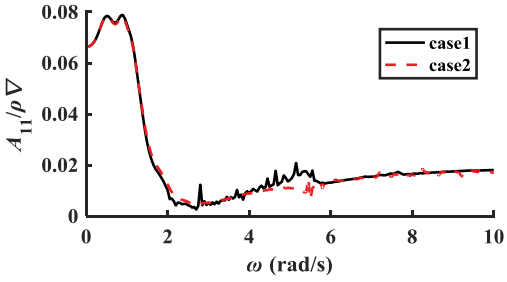

(a) The 1st mode

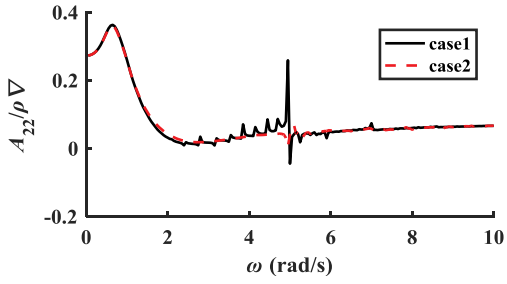

(b) The 2nd mode

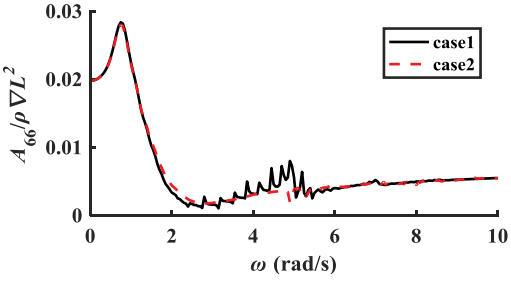

(c) The 6th mode

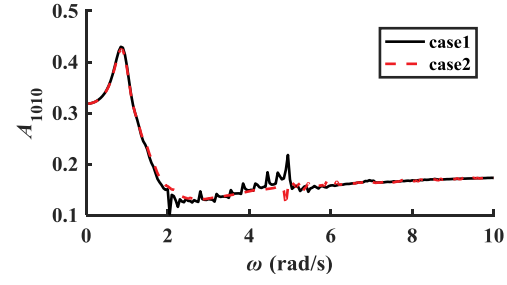

(d) The 10th mode

Fig. 11. Added mass of each mode (infinite water depth).

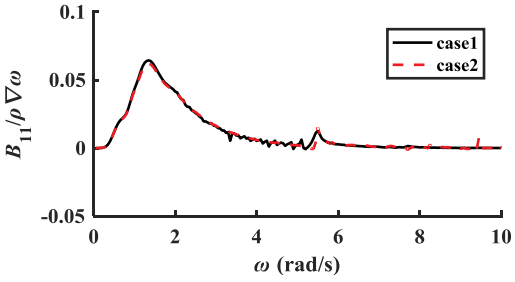

(a) The 1st mode

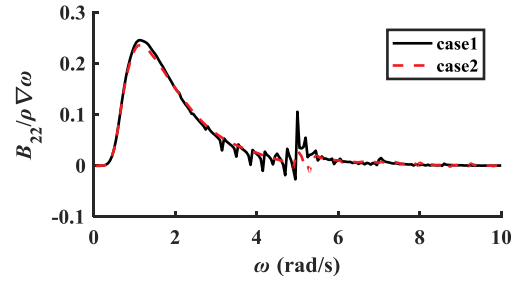

(b) The 2nd mode

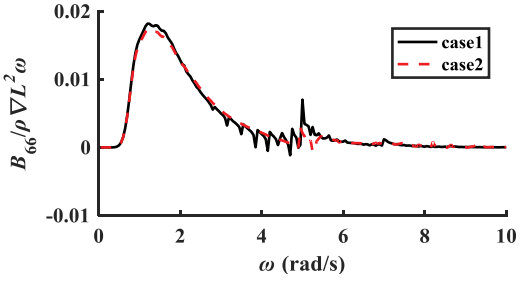

(c) The 6th mode

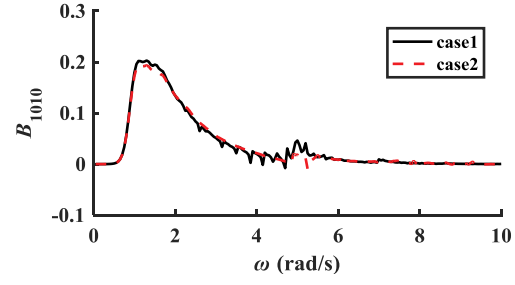

(d) The 10th mode

Fig. 12. Added damping of each mode (infinite water depth).

strength $\phi(Q)$ of the free surface are unknown variables. $\frac{\partial\varphi(P)}{\partial n_e(P)}$ denotes the normal velocity of the wetted surface, also called the generalized normal boundary condition a_r, which is a known variable.

After the source strengths $\sigma(Q)$ and $\phi(Q)$ are solved by Eqs. (19a) and (19b), the velocity potential $\varphi(P)$ of the wetted surface can be obtained by the first formula of Eq. (18).

3.4. Numerical method of solving equation

Assuming that the panel numbers of the wetted surface and inner free surface (also called the rigid lid), are N and M, respectively, the numerical discretization scheme of Eqs. (19a) and (19b) is:

Table 4
The principal parameters of the bulk carrier.

Parameters	Value
L_{BP} (m)	295.0
Broad (m)	50.0
Depth (m)	24.7
Forward draft T_f (m)	17.71
After draft T_a (m)	18.73
Displacement Δ(t)	235610.1
Forward speed	14.8 (Kn)
Water depth (m)	200.0

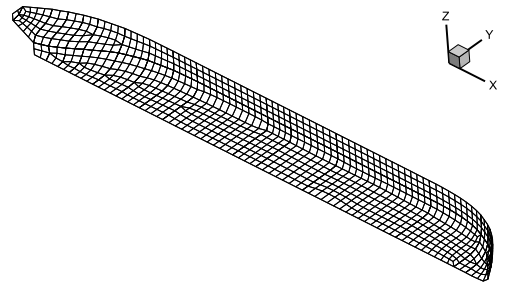

(a) Mesh on hull

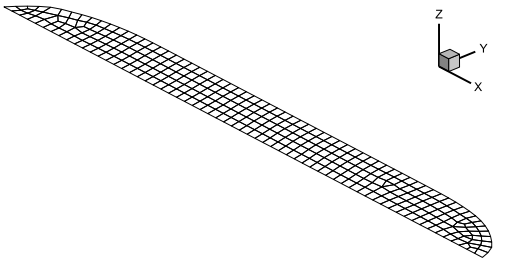

(b) Mesh on rigid lid

Fig. 13. Hydrodynamic model of the bulk carrier in the hydroelastic analysis (half model).

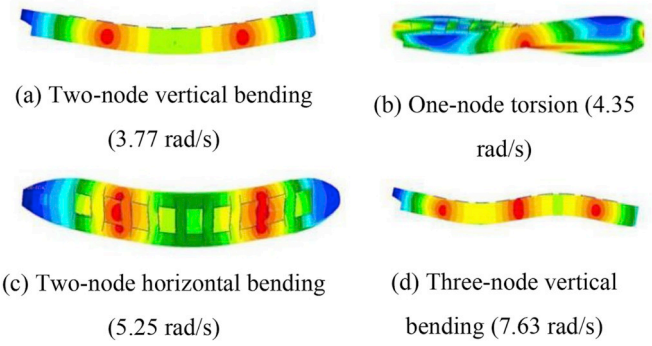

(a) Two-node vertical bending (3.77 rad/s)

(b) One-node torsion (4.35 rad/s)

(c) Two-node horizontal bending (5.25 rad/s)

(d) Three-node vertical bending (7.63 rad/s)

Fig. 14. Dry modal shapes of the bulk carrier.

Table 5
Dry natural frequencies and wet resonance frequencies.

Type	Dry natural frequency (rad/s)	Wet resonant frequency (rad/s)	Experiment Result (rad/s)
Heave	–	0.55	–
Roll	–	0.51	–
Pitch	–	0.60	–
Two-node vertical bending ($f_{2\text{-VB}}$)	3.77	2.80	2.70
One-node torsion ($f_{1\text{-TN}}$)	4.35	4.03	–
Two-node horizontal bending ($f_{2\text{-HB}}$)	5.25	4.57	–
Three-node vertical bending ($f_{3\text{-VB}}$)	7.63	5.53	–

$$\begin{bmatrix} \mathbf{A}_{N\times N} & \mathbf{B}_{N\times M} \\ \mathbf{C}_{M\times N} & \mathbf{D}_{M\times M} \end{bmatrix} \begin{Bmatrix} \sigma_{N\times 1} \\ \phi_{M\times 1} \end{Bmatrix} = \begin{Bmatrix} \dfrac{\partial \varphi}{\partial n_e}_{N\times 1} \\ 0_{M\times 1} \end{Bmatrix} \tag{20}$$

and

$$\mathbf{A}_{PQ} = \begin{cases} 0.5 & , \quad P = Q \\ \dfrac{1}{4\pi} \dfrac{\partial G}{\partial n_e(P)} \Delta S_Q & , \quad P \neq Q \end{cases} \tag{21a}$$

$$\mathbf{B}_{PQ} = \frac{1}{4\pi} \frac{\partial G}{\partial n_e(P)} \Delta S_Q \tag{21b}$$

$$\mathbf{C}_{PQ} = \frac{1}{4\pi} \frac{\partial G}{\partial n_e(P)} \Delta S_Q \tag{21c}$$

$$\mathbf{D}_{PQ} = \begin{cases} -1 & , \quad P = Q \\ \dfrac{1}{4\pi} \dfrac{\partial G}{\partial n_e(P)} \Delta S_Q & , \quad P \neq Q \end{cases} \tag{21d}$$

where the diagonal coefficients of [**A**] and [**D**] are 0.5 and −1.0, respectively.

4. Verification and analysis of the results

4.1. Barge

To validate the influence of irregular frequencies and the elimination method adopted in the paper, one rectangular barge is taken as the research object. The main scales of the barge are shown in Table 1. As the barge exhibits mirror symmetry about the X-Z plane, the left half of the hydrodynamic model is used, which is shown in Fig. 5 (a). The panel number of the half hydrodynamic model is 448 for the barge. To eliminate the irregular frequencies, three kinds of rigid lids are introduced, as shown in Fig. 5 (b) ~ (d), with mesh sizes of 6m × 6m(51 panels), 3m × 3m(170 panels), 2m × 2m(350 panels), respectively. Six cases are considered for the water depth and the influence of the panel size of the rigid lid, as shown in Table 2.

A 3D FEM model of the barge in vacuum is used to calculate the dry global modes and corresponding dry natural frequencies. Fig. 6 shows the modes of the two-node vertical bending, one-node torsion, three-node vertical bending, and two-node horizontal bending with dry natural frequencies from 3.0 rad/s to 4.0 rad/s. Then, four structural elastic modes are involved in the hydroelastic response analysis. The wet resonance frequencies in the fluid are calculated by Eq. (14), as shown in Table 3. It is concluded that the vibration frequencies of the barge in the fluid are obviously reduced. The artificial viscous damping ratio is 3% for heave, roll and pitch and zero for the other modes. The wave direction is 45°.

The irregular frequencies of the barge are calculated theoretically by Eq. (15), which are 1.990, 1.994, 2.002, 2.015, …rad/s. Obviously, the irregular frequencies predicted by the above equation become closer to each other when m and n are large.

For the case of a 10 m water depth, the added mass and added damping of all modes are shown in Fig. 7 and Fig. 8; meanwhile ρ, ∇ and a denote the fluid density, displacement volume and wave amplitude, respectively. The numerical results show that the first irregular frequency appears at 2.00 rad/s, which coincides with the theoretical result. At the same time, it is concluded that the method adopted in the paper can efficiently eliminate the irregular frequency. The coarse mesh ('rigid lid 1′) can eliminate the irregular frequencies from 2.0 rad/s to 3.0 rad/s, and the finer mesh ('rigid lid 2′) can eliminate the irregular frequencies from 2.0 rad/s to 4.2 rad/s. The finest mesh ('rigid lid 3′) can almost eliminate all the irregular frequencies. It is concluded that the finer the mesh is, the better the result. The mesh ('rigid lid 3′) is fine

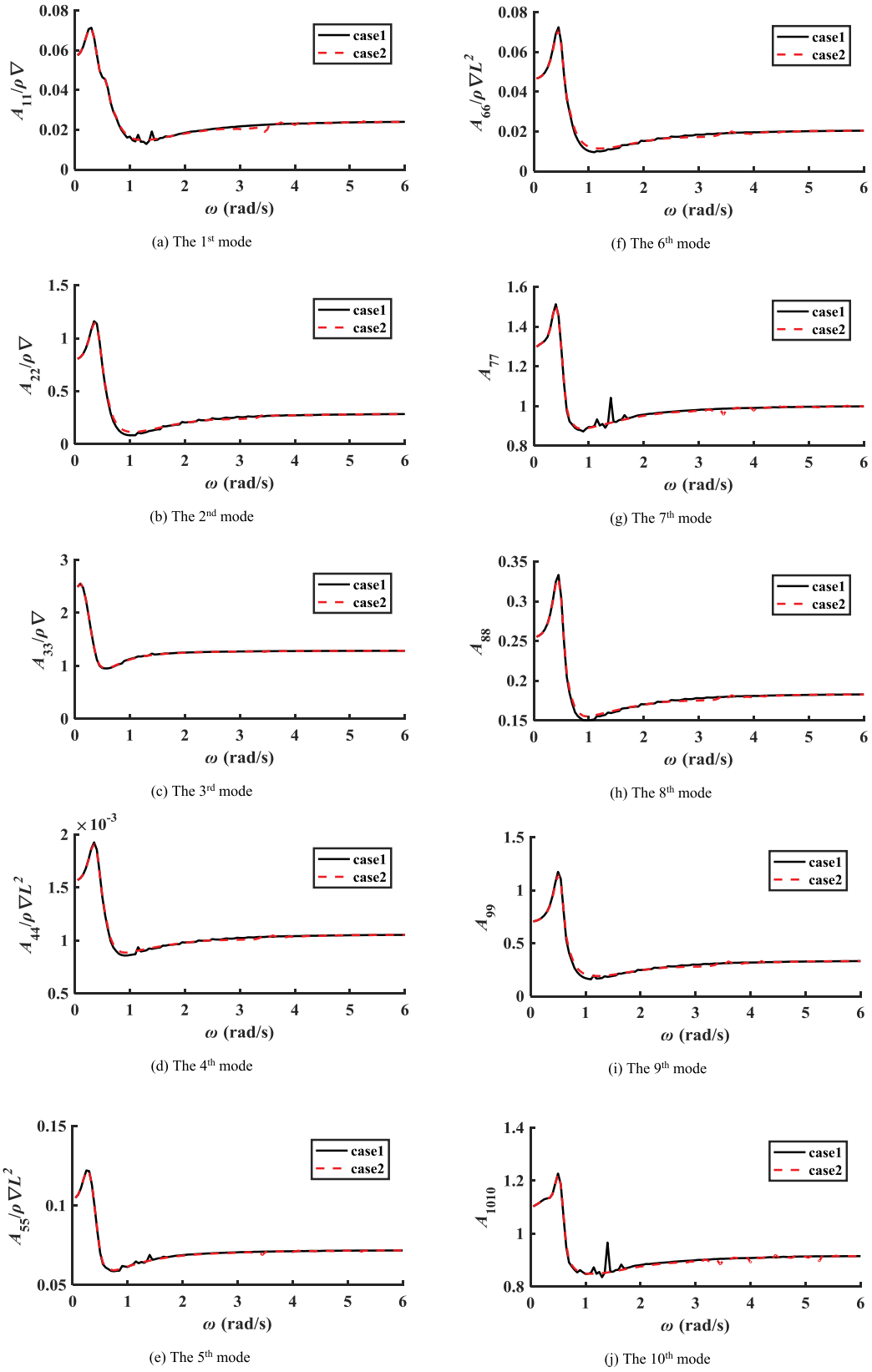

Fig. 15. The added mass of the bulk carrier (infinite water depth).

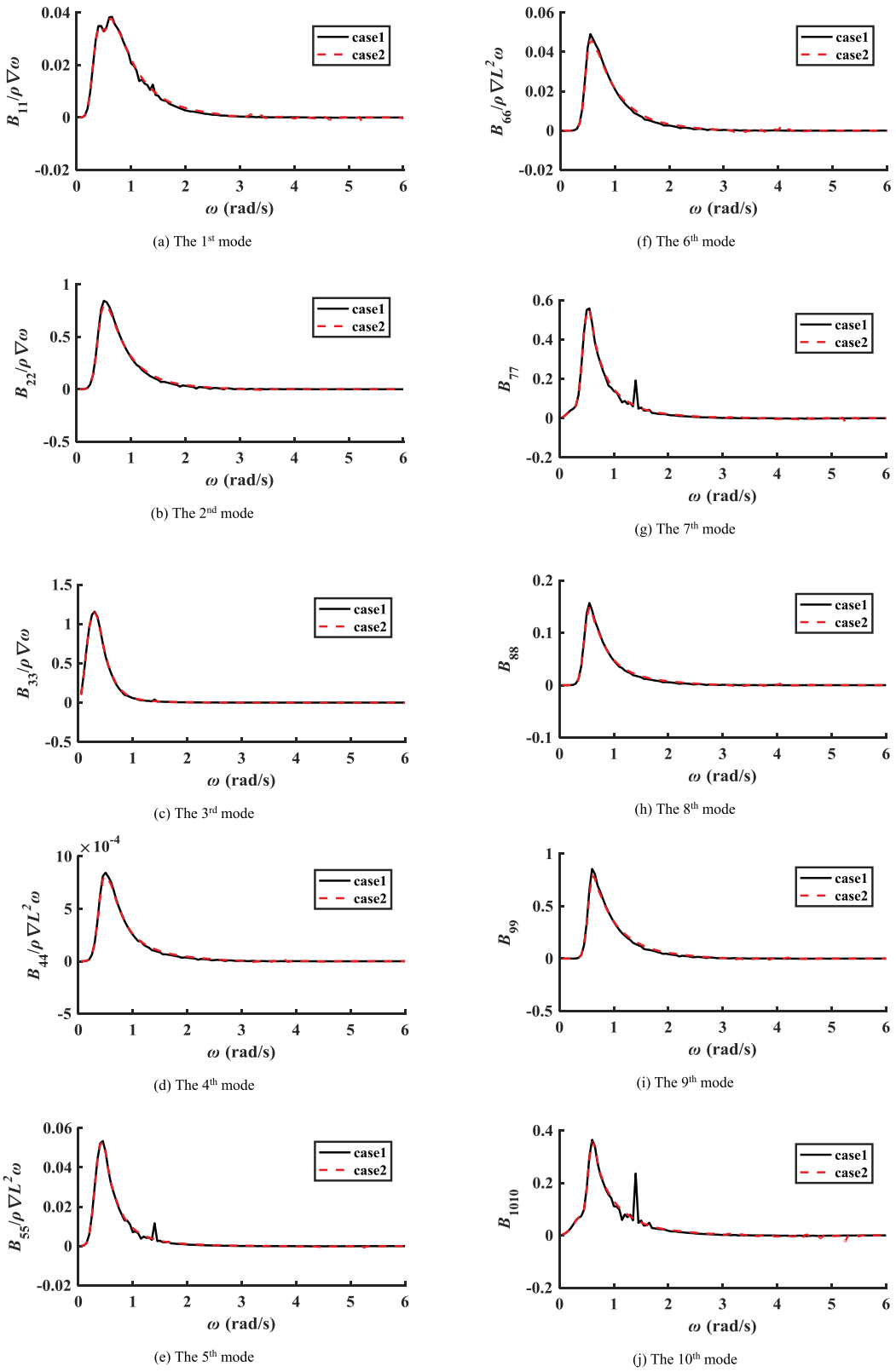

(a) The 1st mode
(b) The 2nd mode
(c) The 3rd mode
(d) The 4th mode
(e) The 5th mode
(f) The 6th mode
(g) The 7th mode
(h) The 8th mode
(i) The 9th mode
(j) The 10th mode

Fig. 16. The added damping of the bulk carrier (infinite water depth).

enough for a numerical assessment of removing irregular frequencies.

Generally, the concerned frequency range is from 0.05 rad/s to 1.5 rad/s for traditional motion and a wave load assessment for rigid floating structures. In this range, there are few irregular frequencies. Therefore, the irregular frequencies only have a small influence on the rigid floating structures. However, for elastic floating structures, such as the barge in the paper, the wet resonance frequencies are from 1.85 rad/s to 3.80 rad/s, which just lie in the range of 2.0 rad/s to 6.0 rad/s with many irregular frequencies. Therefore, it is necessary to eliminate the irregular frequencies for the hydroelastic response analysis, or the

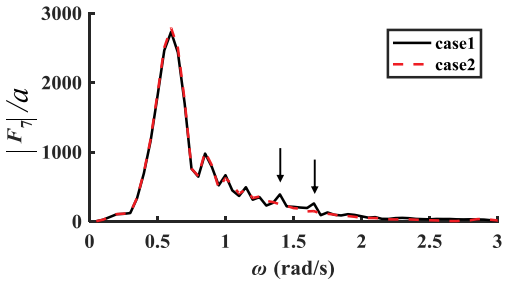

(a) The 7th mode

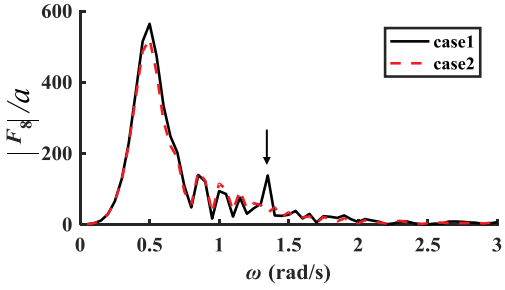

(b) The 8th mode

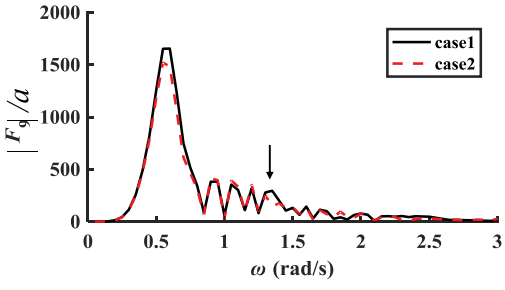

(c) The 9th mode

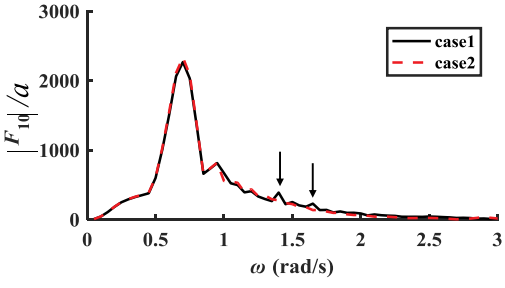

(d) The 10th mode

Fig. 17. Diffraction force of each mode (water depth of 10 m).

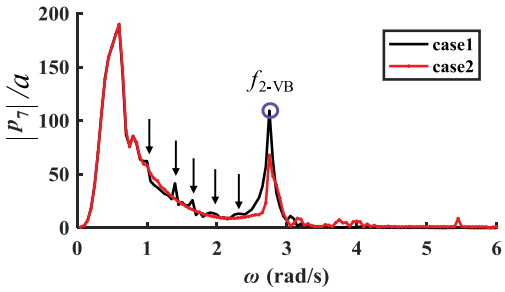

(a) The 7th mode

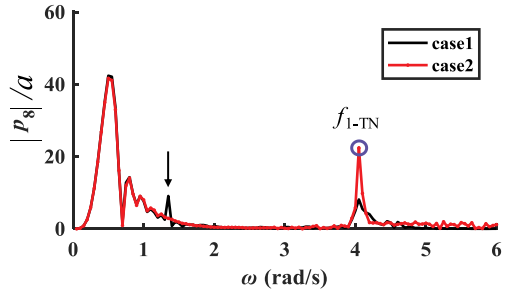

(b) The 8th mode

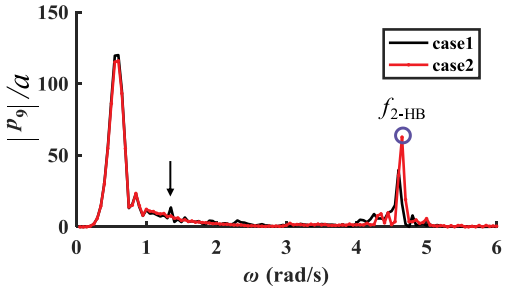

(c) The 9th mode

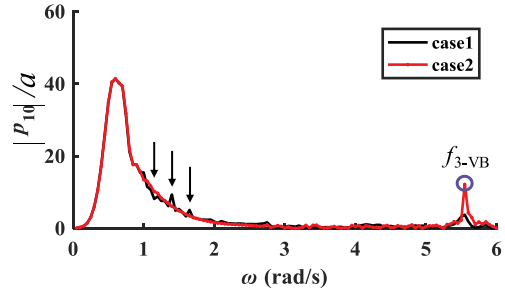

(d) The 10th mode

Fig. 18. The principal coordinate responses of the bulk carrier (elastic modes, wave direction of 45°).

structural dynamic elastic responses will exhibit distortion, as shown in Fig. 9. The black arrows in Figs. 9 and 10 indicate the influence. Although the results in Fig. 9 only show a small effect on the elastic mode responses, the diffraction forces of the barge in Fig. 10 from 2.0 rad/s to 6.0 rad/s are almost zero. This causes the elastic principal coordinate responses from 2.0 rad/s to 6.0 to be almost zero, except for the resonance points. Therefore, it is difficult to determine the influence of irregular frequencies on the elastic principal coordinate responses. However, the next results of one bulk carrier show an obvious influence on the elastic principal coordinate responses.

On the other hand, the motion modes in the horizontal direction have more abundant irregular frequencies, such as the surge, sway, yaw and the horizontal bending modes. For a vertical mode, such as the heave, roll, pitch, vertical bending and torsion modes, the irregular frequencies only lie from 2.0 rad/s to 3.0 rad/s. For surge, sway and the horizontal bending mode, the irregular frequencies have an obvious influence from 2.0 rad/s to 6.0 rad/s. The irregular frequencies become very weak for all modes when ω is larger than 6.0 rad/s. Therefore, the numerical results show that the influence of the irregular frequencies decreases rapidly as the frequency increases. Hence, when the frequency is high enough, the influence of the irregular frequencies can hardly be observed. This is particularly helpful for the hydroelastic analysis of a flexible body. Here, the irregular frequency at low frequency range is called the "significant irregular frequency".

To validate the method adopted in the paper for an infinite water depth, the added mass and added damping are shown in Fig. 11 and Fig. 12. To save space, parts of the results are shown in the figures. It is

concluded that the method adopted in the paper can efficiently eliminate the irregular frequency for an infinite water depth. The other conclusions are the same as the cases of a finite water depth.

4.2. Bulk carrier

A bulk carrier with forward speed is considered to validate the influence of irregular frequencies and the elimination method adopted in the paper. The dead weight of the ship is 205,000 tons. The main parameters are shown in Table 4. A model test of the ship under full loading conditions was carried out at the wave basin of the China Ship Scientific Research Center (CSSRC).

The 3D FEM model of the ship hull has 178157 shell elements, 124032 beam elements and 302189 elements in total. The symmetry of the ship allows the hydroelastic responses to be numerically calculated using half of the wetted surface. The half hydrodynamic model of the ship hull and rigid lid are shown in Fig. 13, with panels 794 and 293, respectively. 'case1′ is without the rigid lid, and 'case2′ is with the rigid lid for removing the irregular frequencies. In addition, the artificial viscous damping ratio is 3% for heave, roll and pitch, 1% for all elastic modes, and zero for the other modes. The wave direction is 45°.

The 3D FEM model of the bulk carrier in vacuum is used to calculate the dry global modes and corresponding dry natural frequencies. Fig. 14 shows the modes of the two-node vertical bending, one-node torsion, two-node horizontal bending, and three-node vertical bending with full scale dry natural frequencies from 3.8 rad/s to 7.6 rad/s.

The dry natural frequencies and wet resonance frequencies are as shown in Table 5. The wet resonance frequencies of the elastic modes are from 2.80 rad/s to 5.53 rad/s according to the numerical calculation. The wet resonance frequency of the two-node vertical bending mode is obtained by a hammering test.

The added mass and damping for an infinite water depth are shown in Fig. 15 and Fig. 16; meanwhile, ρ, ∇ and a denote the fluid density, displacement volume and wave amplitude, respectively. The number of irregular frequencies of the bulk carrier is less than that of the barge. The rigid lid has eliminated the influence of irregular frequencies on hydrodynamic coefficients and diffraction forces successfully. With L = 295 m, B = 50 m, and T = 18.1 m, the approximate results of the irregular frequencies calculated by Eq. (15) are 0.775, 0.783, 0.799, 0.874, 0.883, …rad/s. The numerical results in Figs. 15 and 16 show that the first irregular frequency appears at 1.15 rad/s, which is larger than the first frequency of the approximate result. The diffraction forces and elastic principal coordinate responses in Fig. 17 and Fig. 18 are also obviously affected by the irregular frequencies, marked by a black arrow.

Generally, the larger the scale of the floating structure is, the lower the wet resonance frequency for the elastic floating structures; meanwhile, based on Eq. (15), for the larger scale, the irregular frequency has a lower range. Thus, the wet resonance frequencies of Eq. (14) will lie in the range of the low irregular frequencies (also called significant irregular frequencies), and then the elastic responses will be obviously affected by the significant irregular frequencies.

5. Conclusions

The theoretical basis for eliminating irregular frequencies in three-dimensional hydroelasticity is applied by an extended boundary integral method (inherently adding a rigid lid). To validate the feasibility of the adopted method in hydroelasticity and investigate the phenomenon and law of the irregular frequency, one barge and one bulk carrier are taken as research objects. The effectiveness of the method and mesh of the rigid lid are assessed. Some important conclusions are as follows.

(1) The extended integral method adopted in the paper can efficiently eliminate the irregular frequency for an infinite water depth and a finite water depth. The finer the mesh of the rigid lid is, the better the result.
(2) The numerical results show that the influence of the irregular frequencies on hydrodynamic coefficients and diffraction forces decreases rapidly as the responding frequency increases. Hence, when the main responding frequency of hydrodynamic coefficients, diffraction forces and hydroelastic responses is high enough, the influence of the irregular frequencies can hardly be observed. This is particularly helpful for the hydroelastic analysis of a flexible body.
(3) It is quite necessary to eliminate the irregular frequency for large-scale elastic floating structures in the hydroelastic response assessments. Since the wet resonance frequencies will lie in the range of the low irregular frequencies.

Author contribution section

Guarantor of integrity of entire study: Peng Yang, Jingru Li.
Study concepts: Peng Yang, Jingru Li.
Study design: Peng Yang, Jingru Li.
Literature research: Peng Yang, Jingru Li, Wei Zhang.
Experimental studies: Peng Yang, Dongwei Wu.
Data acquisition: Peng Yang, Dongwei Wu.
Data analysis/interpretation: Peng Yang, Jingru Li.
Manuscript preparation: Peng Yang, Jingru Li, Wei Zhang.
Manuscript definition of intellectual content: Peng Yang, Jingru Li, Dongwei Wu, Wei Zhang.
Manuscript editing: Peng Yang, Jingru Li, Dongwei Wu, Wei Zhang.
Manuscript revision/review: Peng Yang, Jingru Li.
Manuscript final version approval: Peng Yang, Jingru Li, Dongwei Wu, Wei Zhang.

Declaration of competing interest

The authors declare that they have no conflicts of interest to this work. We declare that we have no financial and personal relationships with other people or organizations that can inappropriately influence our work, there is no professional or other personal interest of any nature or kind in any product, service and/or company that could be construed as influencing the position presented in, the manuscript entitled.

Acknowledgment

The study is supported by the National Natural Science Foundation of China (51909050).

References

Bishop, R.E.D., Price, W.G., Wu, Y.S., 1986. A general linear hydroelasticity theory of floating structures moving in a seaway. Phil. Trans. R. Soc. Lond. A 316, 375–426.
Du, S.X., 1996. A Complete Frequency Domain Analysis Method of Linear Three-Dimensional Hydroelastic Responses of Floating Structures Travelling in Waves. Ph. D., Thesis. China Ship Scientific Research Center, Wuxi, China.
Du, S.X., Hudson, D.A., Price, W.G., 2011. The occurrence of irregular frequencies in forward speed ship seakeeping numerical calculations. Ocean. Eng. 38, 235–247.
Hu, J.J., Wu, Y.S., Tian, C., Wang, X.L., Zhang, F., 2012. Hydroelastic analysis and model tests on the structural response and fatigue behaviours of an untra-large ore carrier in waves. J. Eng. Marit. Environ. 226 (2), 135–155.
Kleiman, R.E., 1982. On the Mathematical Theory of the Motion of Floating Bodies – an Update. DTNSRDC- 82/074.
Lee, C.H., Newman, J.N., Zhu, X., 1996. An extended boundary-integral-equation method for the removal of irregular-frequency. Int. J. Numer. Methods Fluids 23, 637–660.
Lee, C.H., Sclavounos, P., 1989. Removing the irregular frequencies from integral equations in wave-body interactions. J. Fluid Mech. 207, 393–418.
Liu, Y.J., Falzarano, H., 2019. A wall damping method to estimate the gap resonance in side-by-side offloading problems. Ocean. Eng. 173, 510–518.
Newman, J.N., 1984. An expansion of the osillatory source potential. Appl. Ocean Res. 6 (2), 116–117.

Newman, J.N., 1985. Algorithms for the free-surface Green function. J. Eng. Math. 19, 57–67.
Newman, J.N., 1990. The approximation of free-surface Green functions. In: Wave Asymptotic: Proceeding of the Fritz Ursell Retirement Meeting. Cambridge University Press, pp. 107–135.
Nguyen, H.P., Wang, C.M., Flocard, F., Pedroso, D.M., 2019. Extracting energy while reducing hydroelastic responses of VLFS using a modular raft wec-type attachment. Applied Ocean Research 84, 302–316.
Ni, X.Y., Cheng, X.M., Zhang, Z.W., Tian, C., 2019. Removal of irregular frequencies in 3D hydroelastic analysis and application in ship engineering. Shipbuild. China 60 (1), 69–79.
Ohmatsu, S., 1975. On the Irregular Frequencies in the Theory of Oscillating Bodies in a Free Surface. Papers Ship Res. Inst., No, 48.
Pal, S.K., Datta, R., Sunny, M.R., 2018. Fully coupled time domain solution for hydroelastic analysis of a floating body. Ocean. Eng. 153, 173–184.
Price, W.G., Wu, Y.S., 1984. Hydroelasticity of marine structure. In: The 16th in. Congress of Theoretical and Applied Mechanics (IUTAM). Lyngby, Denmark.
Song, Z.J., Teng, B., 2016. Removing irregular frequency in the pre-corrected FFT method for wave-structure interaction. Chin. J. Hydrodyn. 31 (4), 489–495.
Teng, B., Li, Y.C., 1996. A unique solvable higher order BEM for wave diffraction and radiation. Ocean. Eng. 1, 30–38.
Ursell, F., 1981. Irregular frequencies and the motion of floating bodies. J. Fluid Mech. 105, 143–156.
Wei, W., Fu, S.X., Moan, T., 2018. A time-domain method for hydroelasticity of very large floating structures in inhomogeneous sea conditions. Mar. Struct. 57, 180–192.
Wu, Y.S., 1984. Hydroelasticity of Floating Bodies. Ph.D., Thesis. Brunel University, U.K.
Wu, H.L., Chen, X.J., Shen, H.P., 2019. Experimental and numerical investigation of the hydroelasticity of a floating structure with legs. Marine Structures 61, 100–118.
Yang, P., 2016. 3D Nonlinear Hydro-elastic Response Study of Ships in Time Domain. Ph. D. Thesis. China Ship Scientific Research Center, Wuxi, China.
Yang, P., Gu, X.K., Ding, J., 2018. 3D nonlinear hydroelastic response and load prediction of a large bulk carrier in time domain. Journal of Ship Mechanics 22 (12), 1495–1507.
Zhang, X.T., Lu, D., Gao, Y., 2018. A time domain discrete-module-beam-bending-based hydroelasticity method for the transient response of very large floating structures under unsteady external loads. Ocean. Eng. 164, 332–349.
Zhu, X., 1994. Irregular Frequency Removal from the Boundary Integral Equation for the Wave-Body Problem. M.S. Thesis. Department of Ocean Engineering, MIT, Cambridge, MA.